Journal of Nuclear Materials 394 (2009) 123–130

Contents lists available at ScienceDirect

Journal of Nuclear Materials

journal homepage: www.elsevier.com/locate/jnucmat

Computation of free-molecular flow in nuclear materials

Andrew M. Casella [a,b,*], Sudarshan K. Loyalka [a,*], Brady D. Hanson [b]

[a] Nuclear Science and Engineering Institute and Particulate Systems Research Center, University of Missouri-Columbia, Columbia, MO 65211, USA
[b] Radiochemical Sciences and Engineering Group, Pacific Northwest National Laboratory, Richland, WA 99352, USA

ARTICLE INFO

Article history:
Received 31 March 2009
Accepted 11 August 2009

ABSTRACT

Generally, the transport of gases and vapors in nuclear materials is adequately described by the diffusion equation with an effective diffusion coefficient. There are instances however, in which the flow pathway can be so restrictive that the diffusion description has limitations. In general, molecular transport is governed by intermolecular forces and collisions (interactions between multiple gas/vapor molecules) and by molecule–surface interactions. However, if nano-scale pathways exist within these materials, as has been suggested, then molecular transport can be characterized as being in the free-molecular flow regime where intermolecular interactions can be ignored and flow is determined entirely by molecule–surface collisions. Our purpose in this investigation is to focus on free-molecular transport in fine capillaries of a range of shapes and to explore the effect of geometry on this transport. We have employed Monte Carlo techniques in our calculations, and for simple geometries we have benchmarked our results against some analytical and previously available results. We have used Mathematica® which has exceptional built-in symbolic and graphical capabilities, permitting easy handling of complicated geometries and good visualization of the results. Our computations provide insights into the role of geometry in molecular transport in nuclear materials with narrow pathways for flows, and also will be useful in guiding computations that include intermolecular collisions and more realistic gas–surface collision operators.

1. Introduction

The transport of gases and volatile compounds within and through nuclear and non-nuclear materials used in various nuclear facilities is of great interest in the containment of radioactive contamination. Generally this transport is adequately described by the diffusion equation with an effective diffusion coefficient being determined with empirical methods [1–4]. There are instances however, where the diffusion description has limitations. Such cases occur when the flow pathways through which gases and vapors are moving are so narrow that the interactions of molecules with the pathway walls are as or more important than intermolecular interactions. Although such circumstances are extreme, there are opportunities for them to occur in transport through many media such as nuclear fuels, cladding and coating materials, graphite, rocks, and soil.

In most cases involving materials used in nuclear facilities, species of interest are transported either via solid-state diffusion, or gas phase diffusion and/or convection. However, in a few cases, either the known diffusion and/or convection models fail to adequately describe experimental data, or actual structures in transport media are observed that suggest that continuum transport is questionable. In the first case, traditional models of transport through urania fuel could not properly account for experimental results [5–7]. Additionally, recent experimental studies with respect to transport through silicon carbide coatings [8,9] have suggested that the diffusion equation may be limited in specific circumstances. In the second case, material studies [10–18] have indicated that in some circumstances, physical conditions exist in which the diffusion description cannot be easily applied since the mean free path of molecules is comparable to a characteristic dimension of the flow (pore or crack radius). In these cases, neither solid-state nor gaseous diffusion is dominant, thus limiting the usefulness of standard diffusion coefficients. An explicit example of such a circumstance is the reported presence of cracks with a mean width of 25 nm in nuclear graphite [11,12]. Some of these cracks are identified with widths as small as 5 nm. In order for continuum conditions for transport to exist in such circumstances, the ratio of the mean free path to the crack width should be less than 0.1. The mean free path of gases is determined by [19].

$$\lambda = \frac{k_B T}{\sqrt{2}\pi\sigma^2 p} \tag{1}$$

where λ is the mean free path, k_B is the Boltzmann constant, T is the absolute temperature, σ is the molecular diameter, and p is the

* Corresponding authors. Address: Nuclear Science and Engineering Institute and Particulate Systems Research Center, University of Missouri-Columbia, Columbia, MO 65211, USA. Tel.: +1 509 376 1570 (A.M. Casella).
E-mail addresses: Andrew.Casella@pnl.gov (A.M. Casella), loyalkaS@missouri.edu (S.K. Loyalka).

0022-3115/$ - see front matter © 2009 Elsevier B.V. All rights reserved.
doi:10.1016/j.jnucmat.2009.08.012

pressure. In order for continuum conditions to exist and associated equations to apply in a 5-nm crack, the mean free path must be less than 0.5 nm. Molecular diameters of interest are commonly on the order of 0.3 nm [20]. According to Eq. (1), at standard atmospheric conditions, the mean free path of a gas with a molecular diameter of 0.3 nm is 101.5 nm – making the ratio of the mean free path to the crack radius 4.1 for a crack with a radius of 25 nm or 20.3 for a crack with a radius of 5 nm. Thus, for the cracks described above at standard atmospheric conditions, gas and vapor transport cannot be described by continuum conditions and the associated diffusion equation. If the system described above had a temperature of 700 K and a pressure of 10 MPa, then the mean free path of the gas would be 2.4 nm which is still larger than the required minimum of 0.5 nm.

Generally, fine pathways on the nano-scale do not occur individually, but in vast arrays. This brings about the question as to whether or not the transport of gases and vapors through these arrays may be described with Darcy's Law

$$Q = \frac{-\kappa A}{\mu}\frac{\Delta P}{\Delta L} \tag{2}$$

where κ is the permeability of the porous medium, A is the cross-sectional area for flow, μ is the viscosity of the vapor or gas that is flowing, ΔP is the change in pressure across the medium, and ΔL is the thickness of the medium. However, Darcy's Law applies exclusively to viscous convective flow through a porous medium. In the fine capillary pathways currently being discussed, neither viscous nor convective flow is occurring. Instead, transport is largely being controlled by random thermal motion of the gas or vapor species undergoing transport and by the interaction of these species with pathway walls. As will be shown in this work, for free-molecular flow in fine capillary pathways, a variable W that is analogous to the parameter κ in Darcy's Law can be used to characterize the transport through the pathways. Both parameters function to account for pathway geometry.

As the ratio of the mean free path of the gas or vapor to the crack ratio increases above 0.1, the transition flow regime exists in which molecule–wall collisions become more important and intermolecular collisions become less important. In cases where the ratio of the mean free path to the crack radius is greater than 10, the free-molecular flow regime exists in which intermolecular interactions can be completely neglected. As the free-molecular flow regime is not concerned with intermolecular interactions, modeling of free-molecular transport can be achieved through a Monte Carlo simulation in which molecules travel along straight trajectories between collisions with walls. We should note that even in this regime, computation of the transport is complicated by a general lack of knowledge with respect to the nature of gas–surface collisions (accommodation, condensation coefficients, adsorption, etc.) as well as the geometry of pores and cracks. These complications dictate that computations capable of keeping good fidelity to the actual physical/chemical processes are still some years away.

Our purpose in this investigation is to focus on the free-molecular transport in fine capillaries of a range of shapes and explore the effect of the geometry on this transport. We have used the Monte Carlo method, and for simple geometries benchmarked our results against some analytical and previously available results. We have used Mathematica® due to its exceptional built-in symbolic and graphical capabilities, permitting easy handling of complicated geometries and good visualization of the results. Our computations provide insights into the role of geometry in molecular transport in nuclear materials with narrow pathways for flows, and also will be useful in guiding computations that include intermolecular collisions and more realistic gas–surface collision operators. We should also note that while we have focused here on mass transport, somewhat similar consideration would apply to thermal transport as well.

2. Theory

As mentioned in the introduction, it is common to mathematically describe the movement of materials through fuel matrices and containment materials with a diffusion equation [1,19]

$$\frac{\partial C_A(\underline{r},t)}{\partial t} = D_{AB}\nabla^2 C_A(\underline{r},t) + S_A(\underline{r},t) \tag{3}$$

where C_A represents the concentration of the species that is considered to be diffusing, B is the substance through which species A is diffusing, S_A is the rate of generation by any means of the diffusing species, and D_{AB} is the "diffusivity" or diffusion coefficient that quantifies the rate of diffusion of species A through species B (assumed uniform). We should note that the diffusion coefficient D_{AB} is specifically applicable to a binary diffusion problem (for more complicated problems involving multi-component gas phase transport, a Stefan-Maxwell treatment would be required [19]).

For future discussion it is convenient for us to write Eq. (3) in a more general form:

$$\rho(\underline{r},t)\frac{\partial \omega_A(\underline{r},t)}{\partial t} = -\underline{\nabla}\cdot \underline{j}_A(\underline{r},t) + S_A(\underline{r},t) \tag{4}$$

where ρ is the mass density of the system, ω_A is the mass fraction of the diffusing species, and $\underline{j}_A$ is mass flux. For binary diffusion, this flux is

$$\underline{j}_A(\underline{r},t) = -\rho(\underline{r},t)D_{AB}\underline{\nabla}\omega_A(\underline{r},t) \tag{5}$$

Eq. (5) was derived solely for the description of the steady-state molecular transport via diffusion of one molecular species through another [19]. Such a system is presented in Fig. 1, where species A is represented by the small particles and species B is represented by the large particles. The system consisting of species A and species B is enclosed by a third material (a solid), species C, represented by the brick-like pattern in Fig. 1. Over time, the interactions between the various molecules in the system presented in Fig. 1 will cause the distribution of small particles to become more uniform. It is the nature of the interaction between the molecules in the system that determines the value of the diffusion coefficient in Eqs. (3)–(5).

Consider a modified version of the scenario represented by Fig. 1 in which the large particles (species B) are removed from the system and the enclosing material (species C) is reshaped so that a small pathway or crack exists through which species A can freely "diffuse". This scenario is represented graphically in Fig. 2. In this case, the transport of species A through this pathway is not accurately described by Eqs. (3)–(5). Instead, species A is

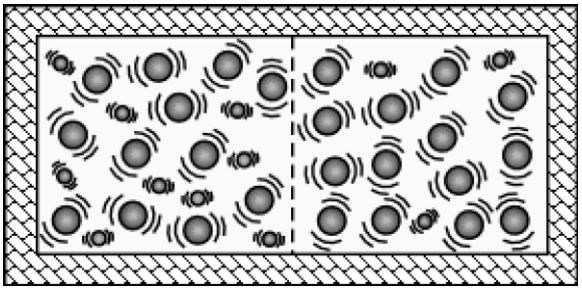

Fig. 1. Representation of a case in which traditional diffusion is described by Eqs. (3)–(5). In this case, species A (small particles) is diffusing from left to right through species B (large particles). The system is enclosed by a third material, species C, which is represented by the brick-like pattern.

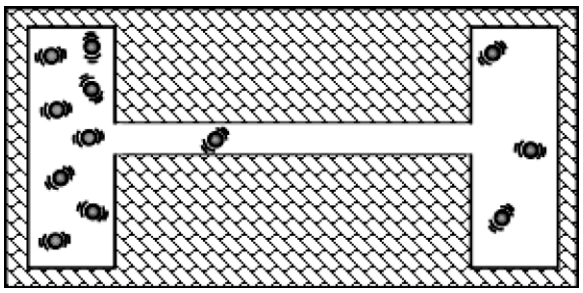

Fig. 2. Transport of molecules of species *A* (small particles) through nano-pathways within species *C* (species *C* is a solid represented by the brick-like pattern).

essentially diffusing through the vacuum within the crack, and D_{AB} does not apply to diffusion of species *A* through a vacuum. In such a situation, another model must be used to more accurately quantify the transport of species *A* through the crack in species *C*.

Determining the flux of a molecular species through a small pathway has been a classic topic of interest in the kinetic theory of gases. Fig. 3 is a simple schematic used as a point of reference for this classic problem. In large part, the focus of previous work on this topic has been on pathways that are straight and have a circular cross-section. The symmetries involved in straight circular pathways allow for analytical treatment of molecular transport through them. A classic summary of theoretical work describing flow of rarefied gases through straight circular tubes of various lengths was created by Clausing, who concluded that free-molecular flow through such a pathway could be described as [21]

$$K_1 = W_1 S_1 I_1 \tag{6}$$

where K_1 is the number of molecules per second traveling through the pathway from the first vessel to the second vessel, S_1 is the cross-sectional area of the entrance to the pathway from the first vessel, I_1 is the number of molecules which in one second strike a unit area of the wall of the first vessel (it is assumed that the pathway connects two vessels, one from which the molecules originate, and one into which they are transferred as shown in Fig. 3), and W_1 is a transmission probability (probability that a given particle that enters the pathway from the first vessel will make it through the pathway to the second vessel instead of being reflected back into the first vessel).

Eq. (6) can be transformed into an equation for mass flux by multiplying it by the molecular mass, *m*, of the molecules being transferred through the tube

$$j_A = mK_1 = mW_1 S_1 I_1 \tag{7}$$

Eq. (7) can be used along with some fundamentals from the kinetic theory of gases to provide a method for predicting the mass flux of a given species through nano-pathways in nuclear materials. From the kinetic theory of gases, it is known that for a given

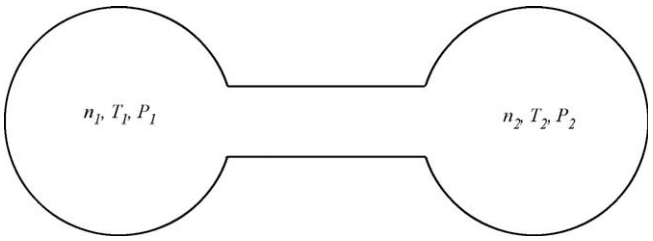

Fig. 3. Schematic used to describe the system of transport for a molecular species from vessel 1 on the left to vessel 2 on the right. Here, n_i represents the number density of the molecules, T_i represents the temperature, and P_i represents the pressure.

system, the number of gas molecules striking a surface of unit area per unit time within a containment vessel is given by the equation [22]

$$I_1 = \frac{n_1 \bar{v}_1}{4} \tag{8}$$

where [23]

$$\bar{v}_1 = \left(\frac{8kT_1}{\pi m}\right)^{1/2} \tag{9}$$

In Eqs. (8) and (9), *n* is the number density of the molecules being transported, *T* is the temperature of the system, and *k* is the Boltzmann constant. Eqs. (7)–(9) can be combined to yield

$$j_A = \frac{1}{4} m W_1 S_1 n_1 \left(\frac{8kT_1}{\pi m}\right)^{1/2} \tag{10}$$

Including transfer of molecules from vessel 2 to vessel 1, the net flow rate becomes:

$$j_A = \frac{1}{4} m W_1 S_1 n_1 \left(\frac{8kT_1}{\pi m}\right)^{1/2} - \frac{1}{4} m W_2 S_2 n_2 \left(\frac{8kT_2}{\pi m}\right)^{1/2} \tag{11}$$

In the case that $T_1 = T_2 = T$, $S_1 = S_2 = S$, and $W_1 = W_2 = W$, Eq. (11) collapses to

$$j_A = \frac{1}{4} m W S \left(\frac{8kT}{\pi m}\right)^{1/2} (n_1 - n_2) \tag{12}$$

If the gradient is explicitly written out for the one-dimensional, scalar version of Eq. (5) describing flow through a system as displayed in Fig. 2 or Fig. 3, the result is

$$j_A = \frac{-mD_A}{L}(n_{A,1} - n_{A,2}) \tag{13}$$

where *L* is the distance between regions 1 and 2 and D_A now represents the diffusion of species *A* through a vacuum as the presence of species *B* has been eliminated. If multiple pathways are present instead of only one, then the mass flux through the system of pathways should equal the right-hand-side of Eq. (12) multiplied by the number of pathways present in the system (assuming all pathways are identical). Such a system would be analogous to a continuous system in which Darcy's Law is applicable as discussed in the introduction.

Eqs. (12) and (13) appear similar to the extent that each is the product of a leading term and the difference in the number density of species *A* between regions 1 and 2. Setting Eq. (12) equal to Eq. (13) and solving for the diffusion coefficient leads to

$$D_A = \frac{1}{4} L W S \left(\frac{8kT}{\pi m}\right)^{1/2} \tag{14}$$

Thus, for a given system, the closer D_{AB} is to D_A, the closer the results from the two approaches will be. In some cases, the results of the two approaches may be indistinguishable. However, in cases where traditional diffusion equations fail, use of Eqs. (10)–(14) may be valuable. If the conditions of a given system are known, then Eqs. (12)–(14) can be used to determine the mass flux through a given pathway. However, the parameter that is almost certainly not known for any given system is *W*, the transmission probability.

3. Modeling

The transmission probability *W* for some simple pathways can be determined analytically [21–27], or numerically [23,28]. The Monte Carlo method has also been used effectively, and a range of useful results have been reported [28–31]. The characteristics of the pathway that must be defined in order to employ such an

algorithm are the pathway geometry, the initial particle trajectory, the nature of intermolecular interactions, and the nature of molecule–wall collisions. In the present work, to focus on the geometrical complexities of the flows, the pathways were assumed small, and intermolecular interactions were neglected. Scattering of molecules from the pathway walls after collisions was considered to be diffuse and thus post-collision trajectories were assigned according to the cosine law [27]. The initial position of a test molecule upon entering the pathway is randomly selected from the cross-section of the pathway entrance. The initial trajectory of the test molecule is also taken from the cosine law. This algorithm was applied to several relatively simple geometries in order to determine the transmission probability W for the pathway. The results provide insights into the role of various geometries in affecting the transmission probability W.

3.1. Straight, right-cylindrical tubes of constant circular cross-section

We follow here an example from Bird [31] closely, and note that Fig. 4 shows the angular entrance parameters that were used to determine the point of entry and the trajectory of each test particle at the beginning of the simulation. The value of φ for each test particle was randomly selected from [0, 2π). The value of θ for each test particle was selected from Eq. (15), which is the cosine law describing a particle that has just recoiled from a collision governed by diffuse reflection [27]. In Eq. (15), the parameter ζ is a random number with a value between 0 and 1. The final parameter value necessary to describe the initial position and trajectory of a test particle is the radial distance from the tube center. In order to make all radial distances equally probable, the value of this parameter was chosen according to Eq. (16), where R is the radius of the tube.

$$\theta = \cos^{-1}(\sqrt{\zeta}) \tag{15}$$

$$r = R(\sqrt{\zeta}) \tag{16}$$

Particles were assumed to follow straight trajectories described by

$$\{x, y, z\} = \{x_0, y_0, z_0\} + \{u_0, v_0, w_0\}t \tag{17}$$

where x_0, y_0, z_0 are the initial spatial coordinates of the test particle and u_0, v_0, w_0 are the initial velocity components of the test particle. For the current simulations, the directional properties of the velocity are important, but the actual magnitude of the velocity is irrelevant since the desired result is only the transmittance and not the time associated with it. At any given time during the test, the distance of the test particle from the central axis of the tube is given by Eq. (18), where it is assumed that the tube central axis is aligned with the x-axis. A particle–wall collision is determined to have occurred when the value of the parameter δ in Eq. (18) equals the radius of the tube.

$$\delta = \sqrt{(y_0 + v_0 t)^2 + (z_0 + w_0 t)^2} \tag{18}$$

After a particle–wall collision, it is necessary to determine the new trajectory of the particle. Since diffuse scattering is assumed, it is necessary that the chosen trajectory be consistent with the cosine law. The first step in assigning such a trajectory is to construct an inward-pointing unit vector that is normal to the wall at the point of impact. For the case currently under consideration, this vector is constructed by placing its tail on the point of impact $\{x_c, y_c, z_c\}$ (where the subscript "c" refers to "collision"), placing its head on the point $\{x_c, 0, 0\}$, and dividing the vector magnitude by the radius of the tube. This translates mathematically into

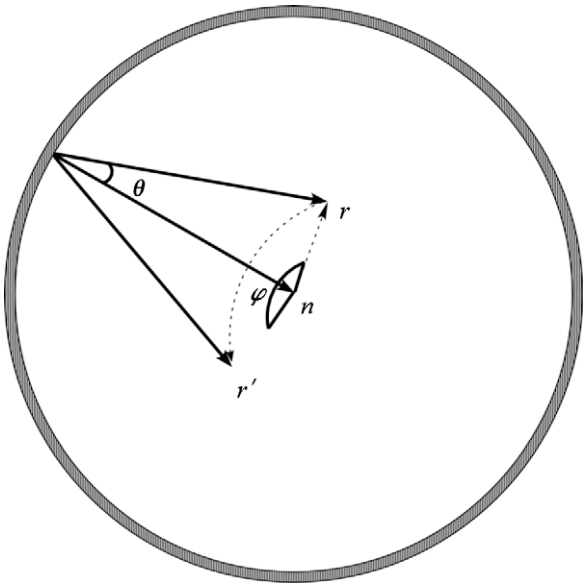

Fig. 5. Post-collision trajectory determination.

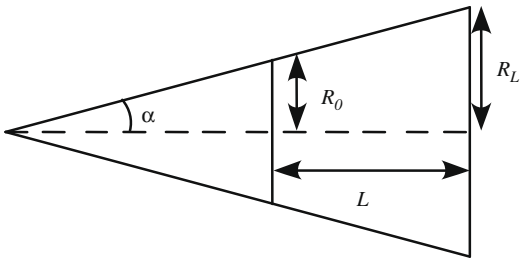

Fig. 6. Conical tube parameters.

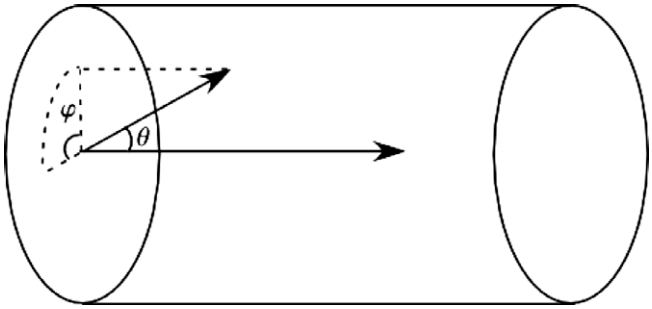

Fig. 4. Angular entrance parameters θ and φ.

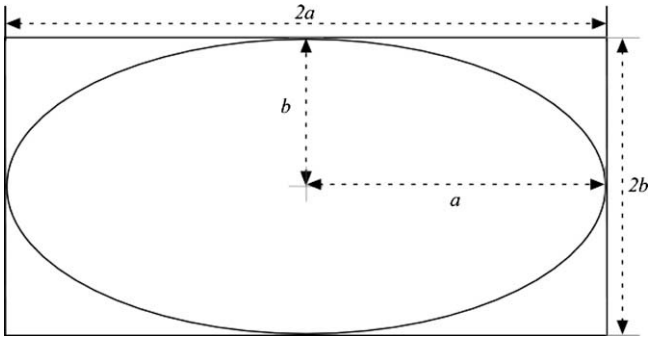

Fig. 7. Important parameters associated with an elliptical tube.

$$\underline{n} = \frac{\{x_c, 0, 0\} - \{x_c, y_c, z_c\}}{R} \tag{19}$$

The post-collision trajectory of the test particle is determined by subsequent rotations along angular parameters analogous to those shown in Fig. 4. Fig. 5 shows the orientation of these parameters as applicable to the description of post-collision trajectory determination.

The inward-pointing unit normal vector $\underline{n}$ is rotated in the radial plane by an angular value of θ that is selected according to Eq. (15). This rotation is performed with the aid of the rotation matrix [32]

$$R_x(\theta) = \begin{pmatrix} 1 & 0 & 0 \\ 0 & \cos\theta & -\sin\theta \\ 0 & \sin\theta & \cos\theta \end{pmatrix} \tag{20}$$

The rotation of the unit vector, $\underline{n}$, by $R_x(\theta)$ results in the vector $\underline{r}$ that appears in Fig. 5. The vector representing the desired post-collision trajectory is then created by rotating the vector $\underline{r}$ according to [33]

$$\underline{r}' = \underline{r}\cos\varphi + \underline{n}(\underline{n}\cdot\underline{r})(1-\cos\varphi) + (\underline{r}\times\underline{n})\sin\varphi \tag{21}$$

Table 1
Visualization of geometries for the helical parameters considered in this study.

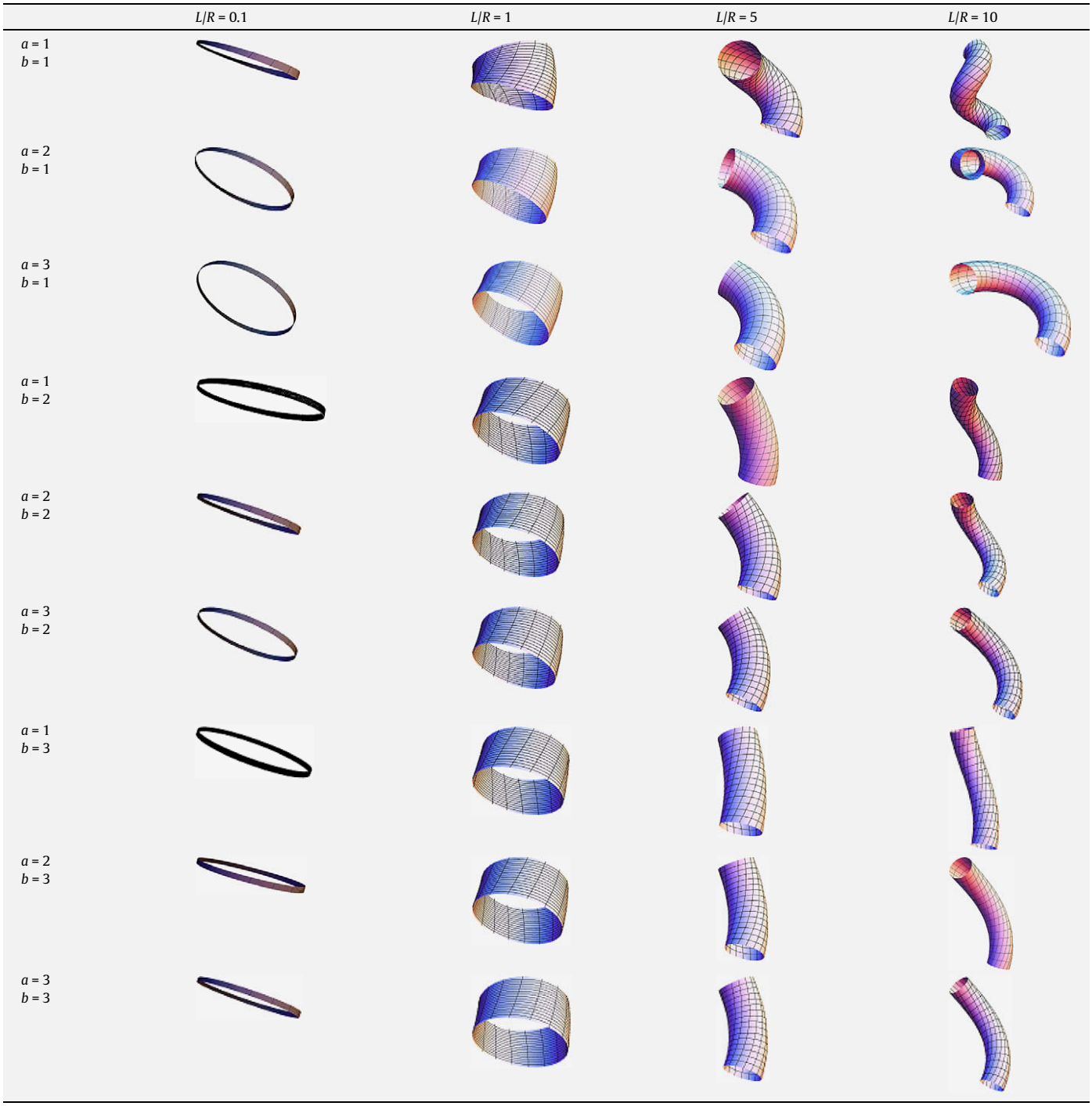

where φ is randomly selected from [0,2π). With the new trajectory, the particle is tracked through collisions until it exits the tube on either side.

3.2. Straight conical tubes

The parameters of interest in tracking particles through a conical tube are displayed in Fig. 6. For the conical tube, initial particle positions and velocities are chosen through the same method used for choosing the initial particle parameters for straight cylindrical tubes. The only difference between these two geometries is that R_0 (the radius of the conical tube at its entrance) is used in place of R. Particle tracking is performed according to the same method as was used for the straight cylindrical tubes except that a particle–wall collision now occurs when $\delta = R(x)$ to accommodate the changing radius of the conical tube. Likewise, the R in Eq. (19) must be replaced by $R(x)$. After $\underline{n}$ is determined according to Eq. (19), it must be rotated by the angle α in the axial direction in order to obtain a unit vector normal to the conical surface at the point of impact. Post-collision particle trajectories are then determined according to the same method used for cylindrical tubes.

3.3. Straight elliptical tubes of constant cross-section

The parameters important for transport through an elliptical tube are shown in Fig. 7. Since the entrance to this tube is not a circle, in order to determine a uniform particle-entrance profile, acceptance/rejection techniques must be employed instead of Eq. (16). The initial particle trajectory is still defined by the cosine law.

Since the elliptical tube does not have a constant radius, determining the location of molecule–wall collisions is more difficult. If the semi-major axis is taken to lie on the y-axis and the semi-minor axis is taken to lie on the z-axis, then a molecule strikes the wall of the elliptical tube when the radial position of the molecule at any axial position is equal to $\{a\cos\theta, b\sin\theta\}$ where θ is the angle between the line segment connecting the molecule position to the tube center {0,0} and the semi-major axis. At any point on the elliptical shell, the unit tangent vector is defined as

$$\underline{T} = \frac{\frac{\partial\{a\cos\theta, b\sin\theta\}}{\partial\theta}}{\sqrt{(a\sin\theta)^2 + (b\cos\theta)^2}} = \frac{\{-a\sin\theta, b\cos\theta\}}{\sqrt{(a\sin\theta)^2 + (b\cos\theta)^2}} \tag{22}$$

Also, if the central curve around which the elliptical tube is constructed lies on the x-axis, then the vector {1,0,0} is a unit vector that is normal to the unit tangent vector defined by Eq. (22). The inward-pointing unit normal vector at the point of impact for a molecule–wall collision is determined from the cross product of this vector with the unit tangent vector. After this inward-pointing unit normal vector is determined, then the same rotation procedure that was used to determine the post-collision trajectory for the molecule in cylindrical tubes is employed.

3.4. Helical tubes with constant circular cross-sections

The unique difficulty characteristic of helical tubes is that the central axis is now three-dimensional and does not correspond to a set coordinate-system axis. The central axis of a helix can be described parametrically as

$$\gamma(a,b,s) = (a\ \cos\ s, a\ \sin\ s, b\ s) \tag{23}$$

where a is the inner radius of the helix, b describes the separation distance between the successive coils of the helix and s is the parametric variable. Due to the fact that the cross-sectional flow area of the helix is a circle, the initial particle conditions that were used for cylindrical and conical tubes can be used for the helix. A molecule–wall collision can be determined to have occurred for flow through a helix when the minimum distance between a molecule and the central curve is equal to the radius (R) of the helical tube. The circular plane cutting perpendicularly through the helix at the point of impact can then be treated as though it were a cross-sectional slice of a cylindrical tube when finding the post-collision trajectories. Due to the curvature of the helical tube, the parameter s does not directly translate into the length of the tube. Instead, the helical length is related to s by

$$L = \int_0^{s_{max}} |\gamma'[s]| ds \tag{24}$$

where γ is defined by Eq. (23). The geometrical parameters of interest for helices are a, b, L, and R (the radius of the tube). Table 1 gives a visual survey of the effects of varying the values of any of these parameters.

4. Results

The results of the various computational experiments described in this paper for the values of W are presented in Tables 2–5. Previously published results for straight cylindrical and conical tubes are presented for comparison in Tables 2 and 3 [21,30]. In Tables 1, 2 and 5, the value L/R is simply the ratio of the tube length to the tube radius. This ratio is defined as L/R_0 in Table 3 for conical tubes where R_0 is the radius at the tube entrance. For elliptical tubes in Table 4, only the value of L is listed since an ellipse doesn't have a "radius." The parameters "a" and "b" used to describe ellipses in Table 4 represent the semi-major and semi-minor axes, respectively as displayed in Fig. 7. For helical tubes in Table 4, the parameters "a" and "b" are defined in Eq. (23).

The computational experiments run in this work used the Monte Carlo method and have associated with them the characteristic relative error associated with this method. The relative error R_{MC} associated with the results of a simulation is defined as [34]

$$R_{MC} = \frac{\sigma_{MC}}{\mu_{MC}} \tag{25}$$

where σ_{MC} is the estimated standard deviation and μ_{MC} is the mean. In order to generate values of the mean and standard deviations, a

Table 2
W and R_{MC} for straight cylindrical tubes.

L/R	Present results	R_{MC} of present results	Results in [21]
0.1	0.9525	0.0024	0.9524
1	0.6701	0.0070	0.6720
5	0.3089	0.0133	0.3146
10	0.1928	0.0178	0.1973

Table 3
W and R_{MC} for straight conical tubes.

	L/R_0	Present results	R_{MC} of present results	Results in [30]
$\alpha = 1°$	0.1	0.9532	0.0019	0.9541
	1	0.6882	0.0066	0.6854
	5	0.3421	0.0153	0.346
	10	0.2322	0.0186	0.2368
$\alpha = 30°$	0.1	0.987	0.0012	0.9869
	1	0.9325	0.0027	0.9334
	5	0.9067	0.0036	0.9081
	10	0.9055	0.0036	0.9061
$\alpha = 60°$	0.1	0.999	0.0004	0.9986
	1	0.9955	0.0007	0.9959
	5	0.9951	0.0007	0.9956
	10	0.9949	0.0008	0.9956

Table 4
W and R_{MC} for straight elliptical tubes.

		L							
		0.1		1		5		10	
	b	W	R_{MC}	W	R_{MC}	W	R_{MC}	W	R_{MC}
$a = 1$	2	0.9606	0.0090	0.7205	0.0059	0.3762	0.0134	0.2427	0.0188
	3	0.9657	0.0075	0.7257	0.0059	0.3990	0.0116	0.2644	0.0172
	4	0.9693	0.0088	0.7590	0.0059	0.4181	0.0111	0.2744	0.0147

Table 5
W and R_{MC} for helical tubes.

		L/R							
		0.1		1		5		10	
	a	W	R_{MC}	W	R_{MC}	W	R_{MC}	W	R_{MC}
$b = 1$	1	0.9518	0.0019	0.6690	0.0045	0.2903	0.0060	0.0332	0.0069
	2	0.9559	0.0021	0.6802	0.0038	0.2807	0.0045	0.0284	0.0045
	3	0.9532	0.0019	0.6798	0.0039	0.3086	0.0040	0.0345	0.0037
$b = 2$	1	0.9529	0.0023	0.6729	0.0047	0.3082	0.0054	0.1841	0.0051
	2	0.9481	0.0022	0.6690	0.0039	0.3047	0.0045	0.1872	0.0034
	3	0.9530	0.0022	0.6781	0.0039	0.2982	0.0046	0.1764	0.0047
$b = 3$	1	0.9506	0.0018	0.6647	0.0036	0.3005	0.0063	0.1883	0.0052
	2	0.9523	0.0020	0.6729	0.0035	0.3049	0.0040	0.1917	0.0040
	3	0.9519	0.0020	0.6706	0.0036	0.3111	0.0051	0.1881	0.0036

set of simulations composed of the same number of particle histories were run. The relative error is proportional to the number of histories N_{MC} through the relation

$$R_{MC} \propto \frac{1}{\sqrt{N_{MC}}} \tag{26}$$

Eq. (26) can be used to determine a constant of proportionality that can be used to determine the relative error associated with simulations consisting of a large number of histories. The relation thus eliminates the need to run several simulations consisting of a large number of histories in order to determine the mean and the standard deviation associated with the simulation. We note that with relatively few particles (10,000), the Monte Carlo results are in fair agreement with the numerical results obtained through solutions of related integral equations [21,30].

5. Discussion and conclusions

The results for the transmission fraction W presented in Tables 2–5 can be largely explained with geometrical arguments. Geometries that present a higher probability for particle–wall interactions have a lower associated transmission fraction. This claim is most readily seen in the results for straight, circular tubes presented in Table 2. Since there is no change in the cross-sectional flow path through the tube, the only geometrical variant is the length of the tube. The longer the tube, the greater the probability that a test particle will encounter the tube wall while traversing the path enclosed by the tube. Another way to think of it is that a higher number of particle–wall collisions is expected for any test particle flowing through a longer tube than one flowing through a shorter tube.

The same geometrical argument just made for straight cylindrical tubes is also valid for straight conical tubes, as is seen by the results presented in Table 3. The results for conical tubes for which $\alpha = 1$ closely match the results for the corresponding tubes in Table 2, with the expected slight increase in the value of the transmission fraction. As expected, this increase becomes more pronounced as the value of α becomes larger. This is because as the value of α increases, there is a lower probability of molecule–wall interactions, and the unit normal to the wall at a point of impact is biased in a direction that promotes transmission.

Elliptical tubes follow the same trend, for the most part. The length of the tube seems to be the strongest influence on the transmission factor. However, for a given tube length, the transmission fraction determined for an elliptical tube in Table 4 is noticeably higher (except for $r/L \sim b/L = 0.1$) than the transmission fraction determined for the corresponding straight cylindrical tube in Table 2. This increased transmission fraction determined for the elliptical tubes is somewhat misleading. For simplicity, the values of "a" and "b" used in this study were taken to be small integers. However, for the results generated to be directly compared to the results in Table 2, it would be necessary that the cross-sectional areas of the corresponding elliptical and cylindrical tubes be the same. If the length of a tube used in a simulation to generate values for Table 2 and the length of a tube used in a simulation to generate values for Table 4 are the same, then the cross-sectional area of the cylindrical tube in each case will simply be $A_{cs} = \pi r^2 = \pi 1^2 = \pi$. On the other hand, for an elliptical tube with $a = 1$ and $b = 2$, $A_{cs} = 1 \cdot 2 \cdot \pi = 2\pi$. Likewise, for $a = 1$ and $b = 3$, $A_{cs} = 3\pi$, and for $a = 1$, $b = 4$, $A_{cs} = 4\pi$. This increase in the cross-sectional flow area leads to the relatively higher transmission fractions displayed in Table 4. It is curious that an increase in the flow area of 2-, 3-, or 4-fold only slightly increases the transmission fraction when comparing a cylindrical tube to an elliptical tube. Thus, the increase in the aspect ratio of the elliptical tube must offset the increase in cross-sectional flow area.

The most complex geometry considered in this study is the helical tube due to its three-dimensional curvature. The most notable result for the simulations using helical tubes represented in Table 5 is the large decrease in the transmission fraction when moving from a helical tube of length 5 to a helical tube of length 10 when the value of "b" = 1. The reason for this phenomenon is once again geometrical as is readily seen by scanning the images of the helices studied depicted in Table 1.

Molecular transport through various materials is of interest in the nuclear sciences and engineering. The computational experiments presented in this paper provide some insight into how the actual geometry of the matrix through which the molecules are being transported may affect the observed experimental diffusion

coefficients for these systems. Table 5, for instance, gives some quantitative feel for how greatly the length of a helical pathway affects the transmission fraction for tightly bound helices. In our work we used Mathematica® which permitted convenient handling of the geometries we considered, and which would also permit similar convenient handling of more complicated geometries that undoubtedly exist in nuclear materials. Extensions of the present work to include such realistic conditions are currently in progress.

Acknowledgements

This research was performed while Andrew M. Casella was under appointment to the US Department of Energy Nuclear Engineering and Health Physics Fellowship Program sponsored by the US Department of Energy's Office of Nuclear Energy, Science, and Technology. Partial support for this research has also been provided by a US Department of Energy NERI Grant, DE-FC07-07ID14831. We also thank the reviewer of the manuscript for several helpful comments.

References

[1] D.R. Olander, Fundamental Aspects of Nuclear Reactor Fuel Elements, TID26711 P1, ERDA (1976), Available from NTIS.
[2] N.E. Todreas, M.S. Kazimi, Nuclear Systems I, Thermal Hydraulics Fundamentals, Hemisphere, 1990.
[3] G. Melese, R. Katz, Thermal and Flow Design of Helium Cooled Reactors, American Nuclear Society, 1984.
[4] M.M.R. Williams, S.K. Loyalka, Aerosol Science, Theory and Practice with Special Applications to the Nuclear Industry, Pergamon, Oxford, 1991.
[5] M.A. Mansouri, D.R. Olander, J. Nucl. Mater. 254 (1–2) (1998) 22–33.
[6] S.G. Prussin, D.R. Olander, W.K. Lau, L. Hansson, J. Nucl. Mater. 154 (1) (1988) 25–37.
[7] D.R. Olander, Adv. Ceram. 17 (1980) 271–293.
[8] H.J. MacLean, Silver Transport in CVD Silicon Carbide, Ph.D Thesis, Massachusetts Institute of Technology, Department of Nuclear Engineering, Cambridge, Massachusetts, 2004.
[9] H. Nabielek, The Mechanism of Silver Retention in Coated Particle Fuel, Dragon Project, Technical Report DTN/801, OECD High Temperature Reactor Project, Kernforschungsanlage Julich, A.E.E. Winfrith, Dorchester, Dorset, England, 1976.
[10] L.L. Snead, T. Nozawa, Y. Katoh, T. Byun, S. Kondo, D.A. Petti, J. Nucl. Mater. 371 (1–3) (2007) 329–377.
[11] K. Wen, J. Marrow, B. Marsden, J. Nucl. Mater. 381 (2008) 199–203.
[12] A.L. Sutton, V.C. Howard, J. Nucl. Mater. 7 (1) (1962) 58–71.
[13] W. Moller, J. Nucl. Mater. 162–164 (1989) 138–150.
[14] A.A. Haasz, P. Franzen, J.W. Davis, S. Chiu, C.S. Pitcher, J. Appl. Phys. 77 (1) (1995) 66–86.
[15] G. Federici, C.H. Wu, J. Nucl. Mater. 186 (2) (1992) 131–152.
[16] A. Hassanein, B. Wiechers, I. Konkashbaev, J. Nucl. Mater. 258–263 (1998) 295–300.
[17] P.J. Hacker, G.B. Neighbour, B. McEnaney, J. Phys. D: Appl. Phys. 33 (8) (2000) 991–998.
[18] R. Schneider, A. Rai, A. Mutzke, M. Warrier, E. Salonen, K. Nordlund, J. Nucl. Mater. 367–370 (2007) 1238–1242.
[19] R.B. Bird, W.E. Stewart, E.N. Lightfoot, Transport Phenomena, second ed., John Wiley & Sons, Inc., New York, 2002.
[20] D. Lide, Handbook of Chemistry and Physics, Chemical Rubber Company, 89th ed., 2008–2009, pp. 6–34.
[21] P. Clausing, Über die Strömung sehr verdünnter Gase durch Röhren von beliebiger Länge, Annalen der Physik 404 (8) (1932) 961–989 (in German, English translation, The flow of highly rarefied gases through tubes of arbitrary length, J. Vac. Sci. Tech. 8(5) (1971) 636–646).
[22] L.B. Loeb, The Kinetic Theory of Gases, third ed., Dover Publications Inc., New York, 1961.
[23] I.N. Ivchenko, S.K. Loyalka, R.V. Tompson Jr., Analytical Methods for Problems of Molecular Transport, Springer, Dordrecht, The Netherlands, 2007.
[24] M.V. Smoluchowski, Annalen der Physik 338 (16) (1910) 1559–1570.
[25] S. Dushman, Production and Measurement of High Vacuum, John Wiley & Sons, New York, 1962.
[26] S. Dushman, J. Franklin Inst. 211 (6) (1931) 689–750.
[27] M. Knudsen, The Kinetic Theory of Gases, Some Modern Aspects, third ed., Wiley & Sons, Inc., New York, 1950.
[28] A. Mohan, R.V. Tompson, S.K. Loyalka, J. Vac. Sci. Technol. A 25 (4) (2007) 758–762.
[29] R.P. Iczkowski, J.L. Margrave, S.M. Robinson, J. Phys. Chem. 67 (2) (1963) 229–233.
[30] J. Gomez-Goni, P.J. Lobo, J. Vac. Sci. Technol. A 21 (4) (2003) 1452–1457.
[31] G.A. Bird, Molecular Gas Dynamics and the Direct Simulation of Gas Flows, Oxford University Press, Inc., New York, 1994.
[32] J.J. Sakurai, S.F. Tan, Modern Quantum Mechanics, revised ed., Addison-Wesley, Reading, Massachusetts, 1994.
[33] H. Goldstein, C.P. Poole, J.L. Safko, Classical Mechanics, third ed., Addison-Wesley, San Francisco, California, 2002.
[34] X-5 Monte Carlo Team, MCNP – A General Monte Carlo N-Particle Transport Code, Version 5, Volume 1: Overview and Theory, LA-UR-03-1987, Los Alamos National Laboratory, Los Alamos, New Mexico, 2005. Available at: http://mcnp-green.lanl.gov/pdf/MCNP5_Manual_Volume_I_LA-UR-03-1987.pdf.